Defining the Global Error of a Multi-Axis Vibration Test

Joel Hoksbergen, Team Corporation, Burlington, Washington

As with most technology, the state of the art for vibration testing is continually advancing. Significant developments in this field have come from both the electronic systems used for control and from the mechanical systems used for excitation. It is becoming commonplace for a modern vibration test laboratory to simultaneously excite multiple degrees of freedom (DOF) of a test article out to 500 Hz or beyond. This relatively new ability for vibration testing raises questions concerning the allowable test tolerances and what comprises an accurate multi-axis vibration test. Difficulties arise in a multi-axis test when one of the excitation DOF has a significantly lower level than the others; in the sense that this DOF is the most difficult to control and often has the largest relative control error. MIL-STD-810G, Method 527, Annex C, discusses this issue in detail and presents a method for considering the overall error of a multi-axis test. This overall, or composite, error is referred to as the "global" error and provides a means to account for differences in excitation levels while maintaining the integrity of the test. This global-error theory is discussed and applied to data collected during a simultaneous three-axis vibration test using special dual Team Corporation Cube Systems with a large bridging test article.

The state of vibration testing is in a transition period. There is growing interest in the vibration testing community in moving from single-axis excitation to multi-axis testing, which gives the ability to replicate a test environment in full six degrees of freedom (six DOF).[1,2] Veterans in the industry liken it to the transition several decades ago from sine vibration testing to the inclusion of random vibration testing. Both electronic control and mechanical excitation systems have made significant strides, making advanced multi-axis control readily available to test laboratories. Multi-axis excitation, often referred to as multiple-input/multiple-output (MIMO) testing, can be used to accurately replicate real-world dynamic environments. Multiple mechanical DOF can be driven simultaneously as any combination of the three translational DOF or the three rotational DOF. This capability allows the test lab the ability to simulate very complex test environments for multi-axis fatigue studies, multi-axis modal analysis and model verification, accelerated life-cycle testing, and product screening.

However, there are many aspects of this transition that are not straightforward. Questions arise about how best to apply legacy standards developed around single-axis testing and how to apply single-axis error tolerances in a logical and practical way. Single-axis standards were developed with a certain level of conservatism built into the profiles, so there are questions as to whether the multi-axis application of single-axis tests result in overtesting the test article. Does the MIMO test then become too extreme? Much of the data used to build the single-axis standards was not developed with multi-axis testing in mind and does not include cross-axis relations between profiles. So what is the best way to combine single-axis standards into a multi-axis test if there is no information relating the cross-spectral density relationship between measurements? Can an algorithm be developed to estimate the cross-spectral densities?

Additionally, there are subtleties in MIMO testing that make the control more difficult than the single-axis case. In multi-axis testing, by definition, there is more cross-coupling between axes. Often, the noise floor is elevated because of this interaction between axes; this can cause issues controlling a low-level profile. Multi-axis testing also has the ability to excite test article nonlinearities between axes that single-axis testing cannot. Should the standard error tolerances be applied without consideration to these subtleties, or does the error of a MIMO test need to be quantified in a different manner? Controlling a test article with closely coupled modes in different axes can also cause difficulties because it is now possible to simultaneously excite both modes and possibly overtest. Should special consideration be given to this test case?

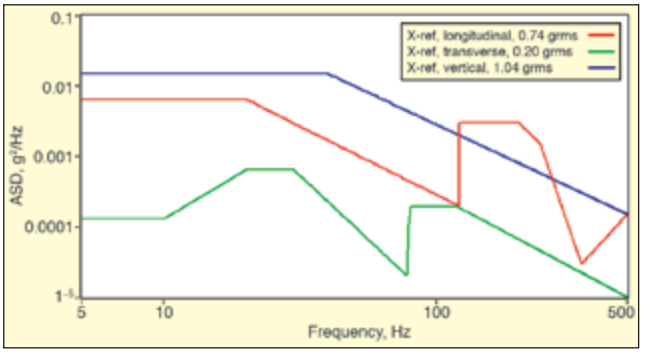

Figure 1. MIL-STD-810G common-carrier test profiles.

Overall, the advantages of MIMO testing vastly outweigh the disadvantages. The questions posed are not insurmountable and simply require detailed discussion and thought among those in the industry interested in accurately replicating six-DOF measurements in the lab. Many organizations and individuals have already begun this analysis. Working Group DTE-022 of IEST is developing a collaborative document on the recommended practices for MIMO testing where many of these questions are addressed.[3] MIL-STD-810G, Method 527, provides a detailed background and summary of the mathematics behind multi-axis vibration testing. Annex C of this document presents an alternative method for defining an allowable error in a MIMO test. It refers to this error as the "global" error of a vibration test.[4] These documents are extremely valuable to the test engineer and provide an excellent background for MIMO vibration testing.

The focus of this article is on applying the global-error algorithm to MIMO systems operating in both multi-axis and single-axis modes. A detailed description is given and applied to two case studies. The subject of the case studies is an advanced MIMO system that dealt with many of the difficulties presented above.

Reason for Quantifying Global Error

The primary reasons for considering a global error is the test case where one or more of the excitation DOF have significantly different auto-spectral density profiles. For example, consider the common-carrier profiles of MIL-STD-810G, Method 514, Annex C, shown in the Figure 1.[5] In this set of profiles, the transverse (Y) axis ranges between one and two orders of magnitude lower than the other two axes. Experience has shown that in the simultaneous MIMO application of these profiles, the Y-axis tends to be the most difficult to control.

Traditional single-axis testing applies an allowable error tolerance of ±3 dB to all of the reference profiles. If the traditional error tolerance were strictly applied to this MIMO test in the bandwidth where the Y-axis profile is two orders of magnitude lower than the Z-axis, a +3 dB deviation of the Y-axis equates to a change from 1% to 2%, relative to the Z-axis. The standard single-axis error tolerance would then dictate that a Y-axis error on the order of 2% of the Z-axis profile would be an unacceptable multi-axis vibration test.

In a MIMO test, one source of error is the cross-axis motion resulting from exciting all three orthogonal axes. Minor errors in the primary axes can translate to significant error on the lowest level profile. Consider Figure 1 as an example, specifically the bandwidth where the difference between the Z and Y axis profiles

is one order of magnitude (10%). If the Z-axis excitation of a MIMO test produced 20% cross-axis excitation on the Y-axis the test would be considered unacceptable because it equates to a +3 dB error on the Y axis (+3 dB of 10%). However, 20% cross-axis motion falls within generally accepted levels for most guided single axis test requirements, and often this is relaxed to 30-40%.[6] Applying this logic to the frequency range where there is a two order of magnitude profile difference, a +3 dB error of the low-level profile (2% cross-axis excitation) would be unacceptable when applying single axis tolerances to the MIMO case, even though guided single axis tests allow 20-40% cross-axis motion of the primary excitation. Given this, it seems unreasonable to hold the control of a low level profile in a MIMO test to the same level of accuracy as the high level X and Z profiles, when that level of accuracy is not required in even the most stringent guided single axis vibration tests. In this example, engineering logic suggests that a better criterion for the allowable error on the Y-axis is needed. For this reason, a Global Error for the MIMO test case is considered.

Auto-Spectral-Density Global Error Algorithm

MIL-STD-810G describes an algorithm for quantifying the global error of a MIMO test in Method 527, Annex C.[4] Hale presented this algorithm at the 77th Shock & Vibration Symposium in 2006.[7] The logic for the algorithm is based in the experience gained from the difficulties previously discussed on trying to simultaneously control a MIMO test with widely different auto-spectral density (ASD) spectra. In this algorithm, a weighting function is developed for each reference profile, which places greater emphasis on the DOF with the highest acceleration levels. The end result is a single-error spectrum that can be used to assess the accuracy of a MIMO vibration test. Method 527, Annex C, describes a method for both MIMO time-waveform replication (TWR) and MIMO ASD random tests. This article deals with the ASD case; however, the TWR algorithm is very similar. The steps for quantifying the global error of an ASD test, according the Method 527, are:

1. Measure the ASD of the control channels during a vibration test.
2. Compile the ASD of the measured control channels and reference profiles into separate matrices.
3. Compute a normalizing factor from the reference profiles at each frequency line.
4. Combine the reference profiles and the normalizing factor into a weighting factor matrix.
5. Calculate the relative error of each measurement channel relative to its reference profile.
6. Normalize the relative error matrix with the weighting matrix.
7. Sum the normalized error matrix components at each frequency line for a global error spectrum.

Applying the Theory

To give some perspective on the application of this algorithm, a case study was conducted on existing data from a MIMO system that Team Corporation developed for a U.S. Navy customer. This system is shown in Figure 2 and was comprised of dual Cube MIMO shaker systems operating as a single six-DOF system to excite a bridging test article. Each Cube uses six internal servo-hydraulic actuators that work as orthogonal pairs to accurately replicate all six degrees of freedom of the payload mounting surface. The actuators provide control over all three translational and rotational DOF of the box structure. The test article was roughly 14 ft. long with an inner isolated mass. The isolation natural frequency was unknown, and the total weight of the article was approximately 3,600 lb. evenly distributed between both Cubes. (See Reference 8 for more details on this system.)

The customer required simultaneous excitation of all three common-carrier profiles shown in Figure 1. Each of the Cubes was controlled using four tri-axial accelerometers located near the base of the test article. All three acceleration measurements at each control point were used for feedback to the vibration controller. So, a total of 24 measurements was used to control 12 independent servo hydraulic actuators and the six DOF of the test article. By definition this is referred to as overdetermined feedback, or rectangular control, in that there are more control points than excitation points.

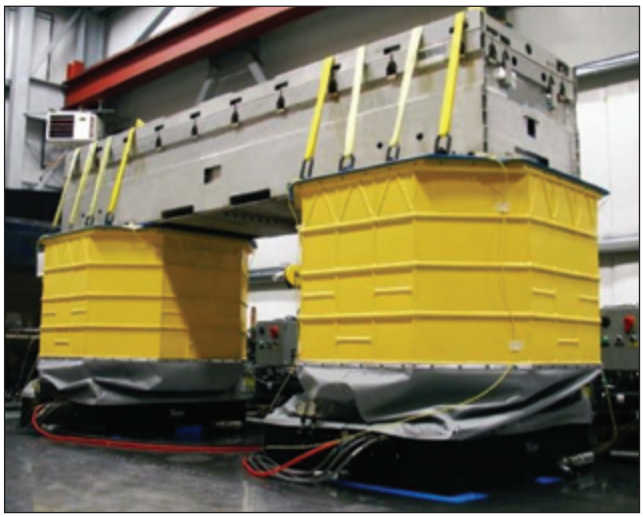

Figure 2. Dual-Cube multi-axis vibration test system.

The common-carrier profiles were set as the reference profiles in the vibration controller for the respective DOF, and the rotational DOF were controlled to a minimum level by defining the allowable phase and coherence levels for the cross-spectral densities (CSD) in the spectral-density matrix (SDM). Assumptions had to be made regarding the CSD, because the test standard does not include this information. Further details on the control of this system are beyond the scope of this article, but there are others that discuss the details of MIMO control.[9-12]

Many of the MIMO difficulties previously discussed were present for this particular test. For example, there was no CSD information between the test profiles, and one of the three profiles was considerably lower than the others. In addition the test used redundant actuators to excite out to 500 Hz the six DOF of a very large test article with closely coupled modes. There also appeared to be non-linearities in the test article structure. In other words, it was an excellent candidate for applying the global-error algorithm. The following sections develop and apply the ASD Global Error algorithm to the data collected on the dual Cube system.

Two cases are considered. First, the global error is calculated for the three-axis simultaneous test to illustrate its usefulness in evaluating the overall performance of a MIMO test. Second, the global error is calculated for the dual Cube system operating in a single-axis configuration. In this case, the setup is still a MIMO test, except that two of the three axes are controlled to a null profile. The latter case considers how the results of the Global Error algorithm compare to the traditional single axis error metric.

Steps 1 and 2: Measure and Compile Data. As with most algorithms, the first step in the global-error algorithm is to measure and compile the data into the appropriate form. The global-error algorithm requires the reference R and laboratory measured L ASD profiles to be compiled into separate matrices of equal size. The algorithm allows for the global error to be calculated using one of the following arrangements:

- Calculate a single global error for all control point measurements.
- Calculate a global error for the measurements at each control point.
- Calculate a global error for the system's six DOF if the coordinate transformation method is used for control.[13]

The key is to be consistent when compiling the data. Given the number of control channels for the case study setup, the global error was calculated at each of the eight control points. The error then accounts for the X, Y, and Z measurement at each point, for a total of eight global-error calculations. The reference and laboratory matrices are $j \times f$-sized matrices, where j is the number of reference/measurement channels and f is the number of frequency lines used to represent each of the ASD profiles.

For the dual Cube, there are three reference profiles defined for each control point, and the data were measured during the test using 400 lines of resolution (ΔF=1.25 Hz), so the two matrices are both 3×400 in size. Equations 1 and 2 show the compilation

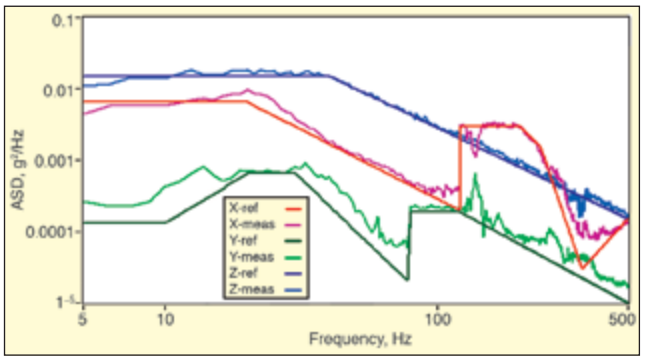

Figure 3. Measurement (laboratory) data vs. reference profiles.

of the reference and measured (laboratory) matrices, respectively. Figure 3 plots the reference profiles and the associated measured data for Control Point 1 on the first Cube. Given the number of measurement points collected in the test, only the data at this first point will be shown in this case study. This point is representative of the error associated with the other points.

$$R_{jxf}\begin{pmatrix} r_{11} & \cdots & r_{1f} \\ \vdots & \ddots & \vdots \\ r_{j1} & \cdots & r_{jf} \end{pmatrix} \tag{1}$$

$$L_{jxf}\begin{pmatrix} l_{11} & \cdots & l_{1f} \\ \vdots & \ddots & \vdots \\ l_{j1} & \cdots & l_{jf} \end{pmatrix} \tag{2}$$

It is clear from Figure 3 that the relative error (the ratio of the measured data to the reference profile at each frequency line) is the largest for the Y axis. In fact, if the ±3-dB lines were plotted, it would show that there are multiple bands where this profile is outside the traditional error tolerance. This plot highlights the difficulty discussed in controlling the lowest level profile.

Steps 3 and 4: Normalizing Factor and Weighting Matrix. Steps 3 and 4 of the algorithm compute a normalizing vector η and use this factor and the reference matrix to generate a weighting matrix W. The normalizing vector is of size $1 \times f$ and can be calculated using one of many normalizing equations. One common function is the L2 norm. This norm is the square root of the sum of the squares. The L2 norm is applied at each frequency line of the reference profiles. Equations 3 and 4 list the normalizing vector and L2 norm, respectively.

$$\eta_{1xf} = \left[\| R_1 \| \quad \| R_1 \| \quad \cdots \quad \| R_f \|\right] \tag{3}$$

$$\| R_1 \| = \sqrt{r_{11}^2 + r_{12}^2 \cdots + r_{1f}^2} \tag{4}$$

Next, the weighting matrix is assembled by calculating the ratio of the square of each component of R and η. Equation 5 shows the assembly of W. It should be noted that the components of the normalizing vector are applied to all components of the associated column of the reference matrix.

$$W_{jxf}\begin{pmatrix} \frac{r_{11}^2}{n_1^2} & \cdots & \frac{r_{1f}^2}{n_1^2} \\ \vdots & \ddots & \vdots \\ \frac{r_{j1}^2}{n_1^2} & \cdots & \frac{r_{jf}^2}{n_f^2} \end{pmatrix} \tag{5}$$

Figures 4 and 5 plot the L2 norm and the weighting matrix for the common-carrier profiles. Comparing the L2 spectrum to the test spectra shows that the L2 norm closely tracks the highest level profile at any given frequency. Plotting the spectra of the individual weighting functions (the rows of W) illustrates the basic premise of the global error algorithm. Over the bandwidths where the Z-axis profile is an order of magnitude higher, or more, than the other profiles, it has a weight that approaches 1.0. Between 120-250 Hz, the X-axis profile has the highest level, and the weighting spectra of the X-axis increases and approaches 1.0 through this bandwidth.

The most interesting observation from the weighting spectra,

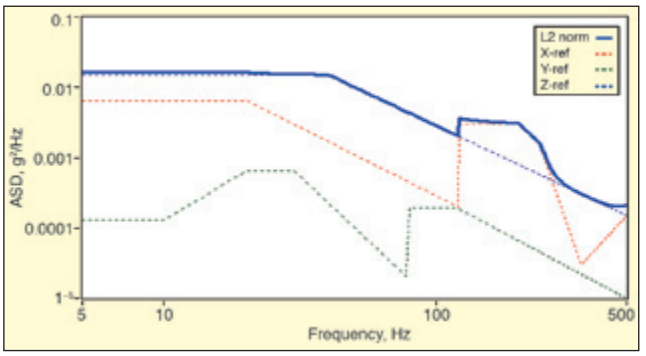

Figure 4. L2 norm of the common carrier profiles.

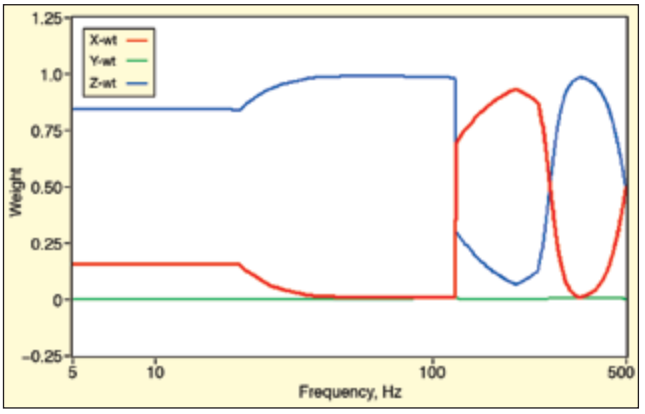

Figure 5. Spectra of weighting of functions for common-carrier profiles.

though, is that the Y-axis spectrum is nominally zero across the full bandwidth, minimizing the emphasis of this axis. One can see that the weighting matrix is a mathematical method for applying the intuitive understanding that the error associated with the Y-axis should not dominate the measure of accuracy for this particular MIMO test, since its level is much lower than the others.

Steps 5 and 6: Relative and Normalized Error. With the weighting matrix known, the relative error can be transformed into a normalized error matrix. The relative error matrix E can be thought of as the traditional error metric that must remain between the ±3-dB tolerance lines during a single-axis vibration test. It is defined to be the ratio of the measured data to the reference profile at each frequency line and for each measurement channel. Often it is preferred to see the error presented in dB, which is included in the definition of Equation 6. The weighting matrix W is then applied to E on a component-wise basis (not matrix multiplication). Equation 7 lists the calculation for the normalized error matrix N:

$$E_{jxf} = 10\log_{10}\begin{pmatrix} \frac{l_{11}}{r_{11}} & \cdots & \frac{l_{1f}}{r_{1f}} \\ \vdots & \ddots & \vdots \\ \frac{l_{j1}}{r_{j1}} & \cdots & \frac{l_{jf}}{r_{jf}} \end{pmatrix} \tag{6}$$

$$N_{jxf} = \begin{pmatrix} E_{11}\cdot W_{11} & \cdots & E_{1f}\cdot W_{1f} \\ \vdots & \ddots & \vdots \\ E_{j1}\cdot W_{j1} & \cdots & E_{jf}\cdot W_{jf} \end{pmatrix} \tag{7}$$

Plotting the relative error and the normalized error on the same scale illustrates the effect of weighting the measurements based on the relative ASD level. Figure 6 plots the relative error for all three measurements across the full bandwidth. The typical single-axis test aims to control this error to within ±3 dB of the reference profile. This plot clearly shows that the Y-axis measurement exceeds the profile by more than +3 dB over several bandwidths, and the X-axis has bandwidths that exceed both the +3 dB and the –3 dB tolerance. The Z-axis, however, maintains good control over most of the profile, with a single error band that approaches the –3 dB tolerance level.

Figure 7 plots the normalized error spectra and highlights the

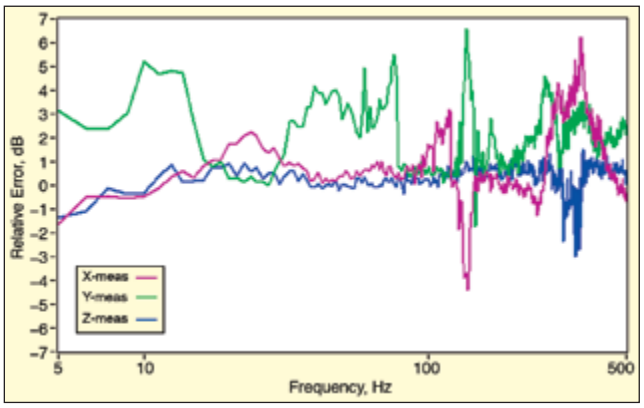

Figure 6. Relative error of each axis for measurement point 1.

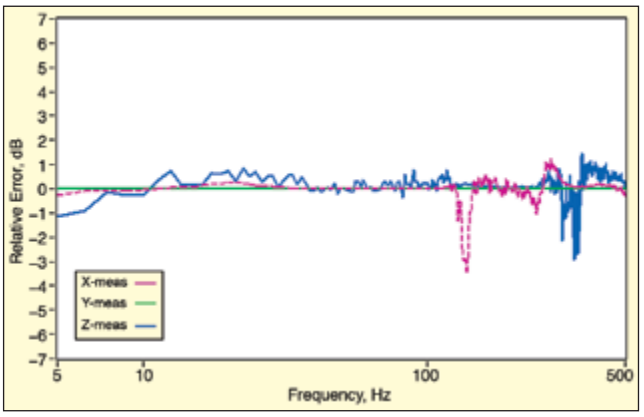

Figure 7. Normalized error of each axis for measurement point 1.

effectiveness of the weighting functions. The normalized error of the Y-axis is nominally zero, and the emphasis has been placed on the high-level profiles. The error in the X-axis that exceeds –3 dB remains in the normalized calculation, because in this particular bandwidth, the X-axis is the highest level profile. However, when the X-axis profile is significantly lower than the Z-axis at the higher frequencies, the normalized error of X is reduced similar to the Y-normalized error.

Finally, the Z-axis normalized error is essentially the same as the relative error. This is to be expected, because the weighting function for Z was close to one for most of the bandwidth (except where the X-axis profile becomes the dominant level). These plots showcase the main objective of the global error algorithm, which is to emphasize the error of the highest-level profile and allow larger errors on the profiles that are considerably lower.

Step 7: Quantify the Global Error. The last step of the global-error algorithm is to quantify a single error metric that can be used to assess the overall accuracy of a MIMO test. This simply entails summing the normalized error components at each frequency line:

$$G_{1xf} = \left[\sum_{i=1}^{j} N_{i1} \quad \cdots \quad \sum_{i=1}^{j} N_{if} \right] \tag{8}$$

Figure 8. Global error vs. Z-axis normalized error. and Figure 9. Global error vs. X-axis normalized error. plot the global error vs. the Z-axis and X-axis normalized error, respectively. These plots show how well the global error tracks the highest-level profile. Where the Z-axis profile is dominant, the global error tracks this normalized error. When the X-axis becomes the dominant profile, however, then the global error follows its normalized error. The end effect is an error metric that places the most emphasis on the high-level profile and allows for larger errors when a profile is considerably lower than the others and is easily influenced by outside excitation sources. The global-error plot can be used as single metric by checking to see that it remains within certain limits (possibly ±3 dB).

Applying the Algorithm to a Single-Axis Test

The ability of the global-error algorithm to account for differences in profile levels when considering a MIMO error metric was shown in the previous case study. In the following section, the global error is applied to data collected on a MIMO vibration system operating in single-axis mode. The data are from the dual-Cube system described previously, exciting only the Y-axis DOF of the test article using the transverse profile from the common-carrier profiles.

In this case, the X and Z axis profiles were defined to be a null level with the intention to perform the test as a single-axis test on a MIMO vibration system. Figure 10 shows the three reference levels for the test setup and the associated measurements for each. It should be noted that the X and Z reference levels were set to be the same level, so only the X reference shows on the plot.

This plot further highlights how the control of a low-level profile can degrade in the simultaneous MIMO case. Now when operating in single-axis mode, the control of the Y-axis is much better than the simultaneous MIMO case, because it is not being adversely effected by the X and Z cross-axis motion. The relative error of Y is well within ±3 dB of the reference, except for some 60 Hz electrical noise and a mode at about 15 Hz. The high response at 15 Hz is most likely due to the mode of the inner isolated mass. Operating the dual Cubes in single-axis mode provided excellent control over the DOF of interest.

Figure 11 plots the relative error of each axis, and it shows that now the X and Z axis error is very large compared to the error of the Y-axis (note the magnitude of the vertical axis). The most likely cause of the large X and Z error is that the reference level is set too low. All systems have a noise level threshold and attempting to control below this level results in large relative errors.[14]

The global-error algorithm was applied to this set of data to see how the error associated with the Y-axis is affected and to consider how the algorithm can be applied to a single axis MIMO vibration test. Figure 12 plots the weighting spectra for the different axes and again highlights how this algorithm places the emphasis on the highest-level profile of a given test and reduces the emphasis of the profiles that are less of a concern, or may not even be considered in a single axis test. Over most of the bandwidth, the Y reference is at least two orders of magnitude higher than the X and Z, except near 500 Hz, where the difference in profiles drops to one order of magnitude. This is reflected in the weighting spectra. The weight of the Y-axis is 1.0 until approximately 400 Hz, since the difference in magnitude between axes decreases.

Figure 13 applies the weights to the relative error and calculates the normalized error spectra of all three axes. This plot shows the Y normalized error to be nominally unchanged from its relative error; however, the normalized errors of X and Z are now effectively zero. This is illustrated by calculating the single global-error spectrum and plotting it against the Y-axis relative error, as shown in Figure 14. In this plot, the global error is essentially identical to the Y-axis relative error, so the global error can be thought of as equivalent to the error that would be measured if the test were conducted on a single-axis vibration test system.

The subtleties of a MIMO test (cross-axis motion and system noise floor) are no longer the emphasis, but rather the error of the DOF of interest becomes the metric of an acceptable vibration test. If this profile were run on a single-axis shaker, most likely the X- and Z-axis responses would not even be measured or considered, and if they were measured, they would likely have a very large relative error. So, the global error is able to frame the MIMO test operating in single-axis mode so that the error metric considered is comparable with what is typically applied to a basic single-axis vibration test. Therefore, the global error algorithm is an effective method for properly quantifying the error of a single-axis test conducted on a multi-axis vibration test system.

Conclusions

As the vibration testing industry transitions to the multi-axis six-DOF testing regime, thought and analysis must be given to various aspects. Properly applying previous standards and considering different ways to quantify an acceptable error are two of these aspects. This article focuses on the definition of the MIL-STD-810G, Method 527, Annex C, global-error metric for MIMO vibration testing. The details of this calculation were detailed and

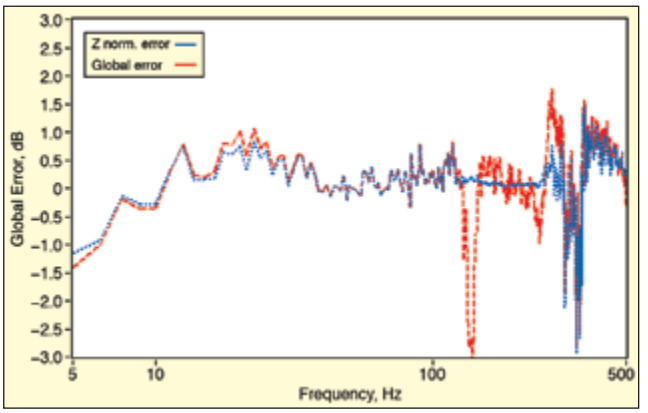

Figure 8. Global error vs. Z-axis normalized error.

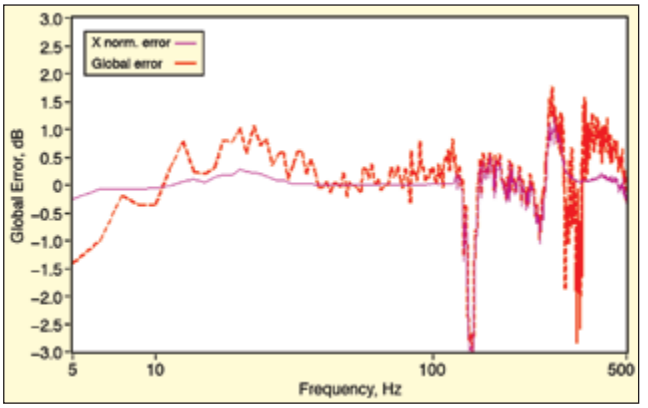

Figure 9. Global error vs. X-axis normalized error.

the algorithm was applied to a set of data collected on a very difficult MIMO test configuration.

The global error discussed is an effective means for placing the emphasis of a multi-axis test on the most highly excited profiles and allowing the error associated with the lower-level profiles to be scaled down according to the difference in magnitude between profiles. The lower-level profiles do not have as large an influence on the excitation of the test article, so it follows that the error of these axes should not dictate satisfactory test acceptance.

In addition to the full six-DOF multi-axis test, the global-error algorithm can be applied to the MIMO system operating in single axis-mode. In this case, the algorithm frames the test in a mathematical way so that the resulting error metric is comparable with what would be measured and achieved on a single-axis system.

The most important aspect of the global-error algorithm is that it uses mathematics to strictly quantify what engineering logic suggests is reasonable, and that is to allow the highest excitation level of a MIMO test to dictate whether measured test results are acceptable.

Acknowledgments

The author would like to acknowledge and thank Dr. Michael Hale of Redstone Test Center, Dynamic Test Division, for his advice and feedback on this article.

References

1. Habtour, E., Connon, W., Pohland, M., Paulus, M., Stanton, S. and Dasgupta, A., "Review of Response and Damage of Linear and Nonlinear Systems under Multiaxial Vibration," Shock and Vibration, Article ID 294271, Vol. 2, 2014.
2. Dasgupta, A., Habtour, E. "Simulation and Test Vibration – Nonlinear Dynamic Effects in Vibration Durability of Electronic Systems," IEEE, 8th International Conference on Integrated Power Electronics Systems (CIPS), Nuremburg, Germany, February, 2014.
3. "Recommended Practice DTE-022, Multi-shaker Test and Control;" IEST, 2014.
4. MIL-STD-810G, Department of Defense Test Method Standard, "Method 527.1, Multi-Exciter Test, Annex C," October 31, 2008.
5. MIL-STD-810G, Department of Defense Test Method Standard, "Method 514.6 Vibration, Annex C," October 31, 2008.
6. MIL-STD-810G, Department of Defense Test Method Standard, "Method 514.6 Vibration, Section 4.2.2.4," October 31, 2008.
7. Hale, M. T. "Considerations of Global Error Metrics in the Conduct of MDOF Motion Replication," Proceedings of the 77th Shock and Vibration Symposium. Monterey, CA, November, 2006.
8. Hoksbergen, J. S., and Woyski, W. B. "Structural Developments Improve High-Frequency Vibration Testing on a Cube Multi-Axis System," Proceedings of the 84th Shock and Vibration Symposium, Atlanta, GA, November 2013.
9. Fitz-Coy, N. and Hale, M. T. "On the Use of Linear Accelerometers in Six-DOF Laboratory Motion Replication: A Unified Time-Domain Analysis," Proceeding of the 76th Shock and Vibration Symposium, Destin, FL, November 2005.
10. Smallwood, D. O. "Random Vibration Testing of a Single Test Item with a Multiple Input Control System," Proceedings, Institute of Environmental Sciences, 1982.
11. Underwood, M. A. and Hale, M. "MIMO Testing Methodologies," Proceedings of the 79th Shock and Vibration Symposium, Orlando, FL, November 2008.
12. Underwood, M. A. and Keller, T. "Understanding and Using the Spectral Density Matrix," Proceedings of the 76th Shock and Vibration Symposium, Destin, FL, November, 2005.
13. MIL-STD 810g, Department of Defense Test Method Standard, Method 527.1, Multi-Exciter Test, Annex B, October 31, 2008.
14. Hoksbergen, J. S. "Advanced High-Frequency Six-DOF Vibration Testing Using the Tensor," *Sound & Vibration*, pp. 6-12, March 2013. SV

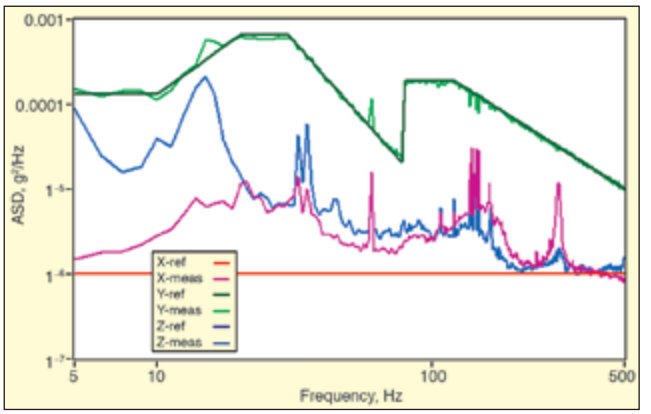

Figure 10. Measured data vs. reference profiles – single axis test.

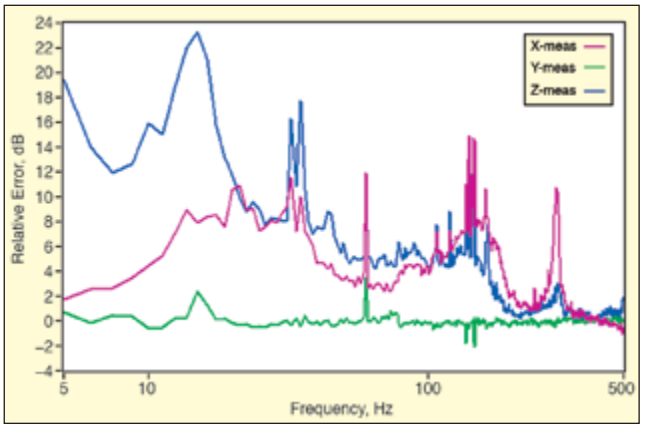

Figure 11. Relative error at measurement point #1 – single axis test.

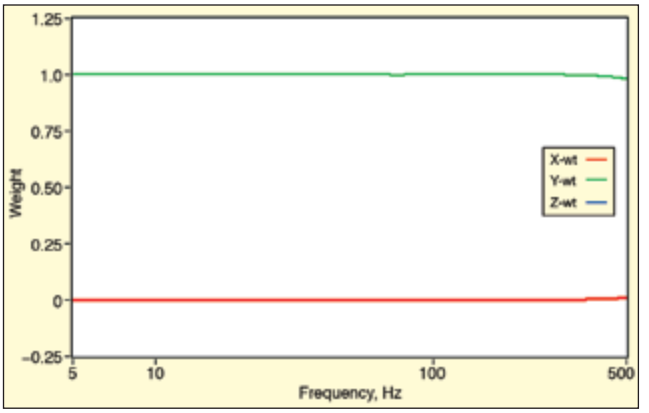

Figure 12. Weighting functions for single-axis test.

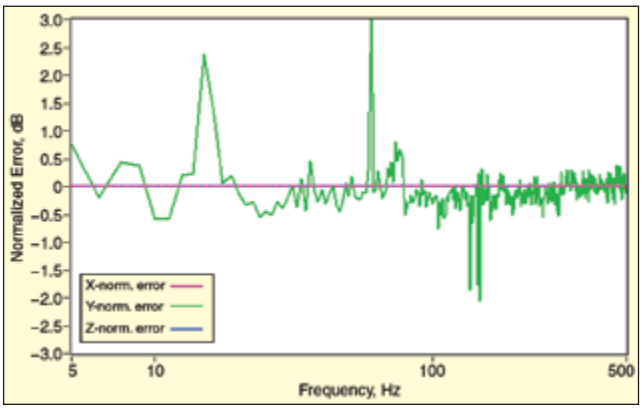

Figure 13. Normalized error at measurement point No.1 – single-axis test.

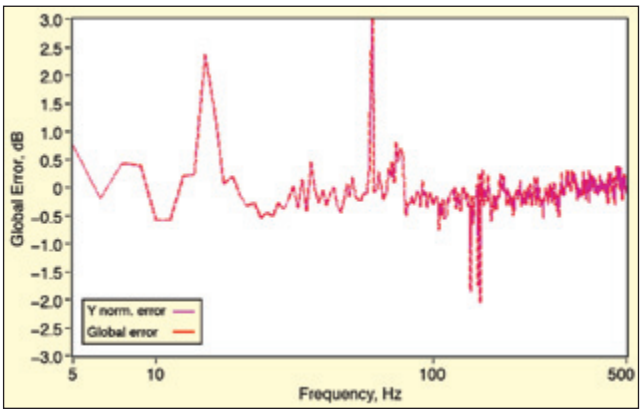

Figure 14. Global error vs. Y-axis normalized error – single-axis test.

The author can be contacted at joel.hoksbergen@teamcorporation.com.